Fracture behaviour of nanobeams through Two-Phase Local/Nonlocal Stress-Driven model

Submitted to **Composite Structures – SI Professor Erasmo Carrera**

August 2021

Version R1, October 2021

FRACTURE BEHAVIOUR OF NANOBEAMS THROUGH TWO-PHASE LOCAL/NONLOCAL STRESS-DRIVEN MODEL

Daniela Scorza[1*], Raimondo Luciano[1], Sabrina Vantadori[2]

[1]Department of Engineering, University of Naples Parthenope, Centro Direzionale Isola C4, 80143 Naples, Italy

[2]Department of Engineering and Architecture – University of Parma Parco Area delle Scienze 181/A, 43124 Parma, Italy

***Corresponding Author:** Daniela Scorza, daniela.scorza@uniparthenope.it

ABSTRACT

The aim of the present work is to employ the two-phase local/nonlocal Stress-Driven integral Model (SDM) to analyse the size-dependent Mode I fracture behaviour of Bernoulli-Euler cracked nanobeams, in terms of energy release rate, stress intensity factor and nonlocal stress field near the crack tip. Both edge- and centrally-cracked nanobeams, subjected to concentrated forces, are examined. The edge-cracked nanobeam is modelled as a pair of cantilever nanobeams, whereas the centrally-cracked nanobeam as a pair of double-clamped nanobeams with internal discontinuity due to concentrated loads. Moreover, a comparison with the results obtained from a gradient elasticity theory based model, available in the literature, is performed. From the present study, it is observed that the energy release rate decreases by increasing the nonlocality, showing the

superior fracture performance of nanobeams with respect to large-scale beams.

KEYWORDS:

Energy release rate, mixture parameter, nanobeam, stress-driven integral model, stress intensity factor

1. INTRODUCTION

The experimental and theoretical investigations of nanomaterials fracture behaviour are topics of great interest for the Scientific Community, since the understanding of the nanoscale fracture mechanisms is critical for tailoring such materials at small length scales **[1,2]**.

Experiments and simulations of fracture at nanoscale level point out the great potential of nanomaterials ultimate strength **[2]**, showing, at the same time, a behaviour significantly different from that exhibited by materials at macroscale level, manifesting the so-called size effect **[3-5]**. Several research works supporting such a statement are available in the literature **[6-10]**. For instance, Fang et al. **[6]** investigated a Gradient Nano-Grained (GNG) surface layer in a bulk Coarse-Grained (CG) rod of a face-centred cubic Cu. It was observed that the tensile yield strength of the GNG/CG was two times greater than that of CG Cu. Wu et al. **[7]** tested a sandwich sheet structure, composed by a CG core between two GNG layers. They observed an extra-strain hardening, with consequent high ductility. Peng at al. **[8]** performed uniaxial tensile tests on single-crystalline copper nanowires by using a micromechanical device inside a scanning electron microscope chamber. They observed that the fracture strength of copper nanowires is much higher than that of bulk copper, and, moreover, that both ductile and brittle-like fracture modes are found in the same batch of fabricated nanowires, depending on their diameters. Le and Batra **[9]** numerically investigated the crack initiation and propagation in pre-cracked single layer graphene sheets under tension by means of molecular dynamics simulations. They found that shorter initial cracks propagated faster than longer ones, but the axial strain registered in the layer with short cracks was higher than in the case of longer cracks. Moreover, Cheng and Sun **[10]**, by adopting the local virial stress in conjunction with molecular dynamic simulations, observed that fracture toughness cannot be treated as a material constant when the crack length is shorter than 100Å. The size-dependent behaviour of fracture toughness was explained by the Authors in terms of the size of the singular stress zone (the K-dominance zone): as the crack length decreases, also the K-dominance zone decreases.

Both the above cited experimental results and numerical simulations highlight that continuum theories, applicable to describe materials behaviour at macroscale level, may not be directly applicable to materials at micro- or nano-scale level, due to the different deformation and fracture mechanisms observed at such a length scale.

In order to capture the small-scale effect on static **[11-18]** and dynamic responses **[12,14,19-25]**, instability **[14,26-28]** and fracture behaviour **[11,29-33]** of nanomaterials at micro- or nano-scale level, several theoretical models have been proposed. Beside them, an innovative method, named Stress-Driven nonlocal integral Model (SDM), is available in the literature **[34-41]**.

The stress-driven nonlocal theory of elasticity assumes that the strains at a point of a body are function of the stresses at all points of the body. Consequently, the elastic strain field is defined by an integral convolution between the elastic stress field and a suitable averaging kernel, and also the associated constitutive boundary conditions are expressed in terms of strains **[34,35]**. The main advantage of the present model is that the elastostatic problem is well-posed, providing analytical results which do not exhibit inconsistencies (due to the swapping of the role of the strain field with that of stress field), avoiding the incompatibility between nonlocal constitutive law and equilibrium requirements as, instead, several Authors highlighted for the well-known Eringen strain-driven model **[42-45]**. The SDM has been recently successfully applied to study nanobeams subjected to bending **[34,35,37]**, axial load **[46]**, torsion **[47]**, buckling **[38-40,48]** and free vibrations **[36,41,49]**.

Moreover, the model has been recently extended by introducing a two-phase local/nonlocal mixture formulation for both free bars under uniform tension, nanobeams under bending loading **[50,51]** and nanobeams under free vibrations **[52]**. Such a two-phase constitutive mixture is defined by a convex combination of both local and nonlocal phases, where the nonlocal fraction is modelled according to the SDM. The aim is to improve the suitability of the stress-driven elasticity theory to model various nanostructures problems.

The novelty of the present paper is to employ, for the first time, the two-phase local/nonlocal Stress-Driven integral Model in conjunction with fracture mechanics concepts in order to analyse the size-dependent Mode I fracture behaviour of the Bernoulli-Euler cracked nanobeams. In particular, the crack opening displacement, the energy release rate, the stress intensity factor and the nonlocal stress field near the crack tip are investigated. Regarding the Bernoulli-Euler nanobeams, two types are examined: an Edge-Cracked Nanobeam (ECN) and a Centrally-Cracked Nanobeam (CCN), both subjected to concentrated forces (Mode I loading). With this aim, the ECN is modelled as a couple of cantilever nanobeams with concentred forces at the free ends, whereas the CCN is modelled as a pair of double-clamped nanobeams with concentred forces at the mid-span section. Consequently, while the local/nonlocal SDM formulation for a cantilever nanobeam is available in the literature **[51]**, an analogous formulation for nanobeams with internal discontinuity due to concentrated loads is here presented for the first time, exploiting the work of Caporale et al. **[53]**.

The paper is organised as follows: the ECN formulation is presented in **Section 2** together with the discussion on the results obtained, whereas the CCN is analysed and the corresponding results are presented in **Section 3**. The nonlocal stress fields near the crack tip in both edge- and centrally-cracked nanobeams are investigated in **Section 4**. Moreover, a comparison between the results obtained and those carried out by using the gradient elastic theory **[54]** is presented in **Section 5**. The main conclusions are, instead, summarised in **Section 6**. Finally, in **Appendix A.1**, the two-phase local/nonlocal SDM formulation is recalled for a cantilever nanobeam, whereas the new formulation for nanobeams with internal discontinuity is presented in **Appendix A.2**.

2. FRACTURE ANALYSIS OF AN EDGE-CRACKED NANOBEAM

2.1 Transversal displacement and CMOD

As in macro-scale models, the fracture behaviour of an Edge-Cracked Nanobeam (ECN), containing a longitudinal crack with a length equal to l (**Figure 1(a)**), may be conveniently modelled by assuming the

crack as a double cantilever nanobeam with length, l, as shown in **Figure 1(b) [55].**

Figure 1

The ECN has a rectangular cross-section with thickness, $2h$, and width, b, and is subjected to a pair of concentrated forces, F, at the free ends. Neglecting the effects of shear, "root-rotation" (crack-tip rotation) and other manifestations of elastic deformation ahead of the crack tip, is acceptable for cracked nanobeams, since their stiffness is higher than that of large-scale beams. Consequently, the elastic deformations ahead the crack tip are lower than in the case of large-scale beams **[56,57].**

The configuration of deformed crack faces under the action of the applied external loads may be analysed by computing the deflection of the two identical single cantilever nanobeams. By taking advantage of the above symmetry, a single cantilever nanobeam is considered (i.e. the upper one in **Figure 1(b)**) and the transversal displacement, $v(x)$, under Bernoulli-Euler assumption, can be written as reported in the following, by applying the two-phase local/nonlocal SDM reported in Ref. **[51]:**

$$v(x)=\frac{Fx^2}{6IE}(3l-x)-(\alpha-1)\frac{FL_c e^{-(x+l)/L_c}}{2IE}\cdot \\ \cdot\left\{L_c^2\left(e^{(x/L_c)}-1\right)\left(e^{(x/L_c)}+e^{(l/L_c)}\right)-xle^{(x+l)/L_c}+L_c\left[-le^{(l/L_c)}-xe^{(x/L_c)}+e^{(x/L_c)}(l-x)\right]\right\} \quad (1)$$

where L_c is the material characteristic length, and IE is the bending stiffness of the single nanobeam; α is the mixture parameter and ranges from 0.0 to 1.0, so that, for $\alpha=0.0$ the fully nonlocal stress-driven model is recovered, whereas for $\alpha=1.0$ the classical Bernoulli-Euler model is obtained. Details regarding the formulation of the local/nonlocal SDM for a cantilever nanobeam, with a concentrated load at the free end, may be found in the **Appendix A.1.**

Consequently, the maximum deflection is attained at the free end (that is, for $x = l$):

$$v_{\max} = \frac{Fl^3}{3IE}\left\{1 - 3(\alpha - 1)\lambda\left[\lambda^2\left(1 - e^{-(1/\lambda)}\right) - \lambda e^{-(1/\lambda)} - \frac{1}{2}\right]\right\} \qquad (2)$$

being $\lambda = L_c / l$ the dimensionless characteristic length (or the dimensionless nonlocal parameter), ranging from 0.0 to 1.0.

The transversal displacement normalised with respect to the maximum deflection value, computed according to the classical local Bernoulli-Euler solution, $v^*(x) = v(x) \Big/ \left(Fl^3 / 3IE\right)$, is plotted against the dimensionless abscissa x/l for different value of α ($\alpha = 0.0,\ 0.2, 0.4, 0.6, 0.8$ and 1.0) and $\lambda = 0.1$ in **Figure 2(a)**.

Figure 2

It is interesting to note the dependency of $v^*(x)$ on the mixture parameter, α. The case with $\alpha = 1$ (thick line) corresponds to the case of the classical Bernoulli-Euler local problem. For smaller value of α, the normalised displacement values are lower, showing a decreasing of about 15% for $\alpha = 0.0$ (fully nonlocal model) in correspondence of $x/l = 1$ (that is, at the free end). Consequently, the nanobeam shows a stiffer behaviour with respect to a large-scale beam.

The Crack Mouth Opening Displacement (CMOD), δ, may be computed as two-times the deflection at the free ends of the double cantilever nanobeam, that is, $\delta = 2v(l)$. Therefore, such a CMOD may be conveniently normalised with respect to the well-known classical local Bernoulli-Euler solution, δ_C, as:

$$\delta^* = \frac{\delta}{\delta_C} = 1 - 3\lambda(\alpha - 1)\left\{\lambda^2\left(1 - e^{-(1/\lambda)}\right) - \lambda e^{-(1/\lambda)} - \frac{1}{2}\right\} \quad (3)$$

with

$$\delta_C = 2 \cdot \frac{Fl^3}{3IE} \quad (4)$$

by explicitly showing the dependence of δ^* on both α and λ.

The normalised CMOD is then plotted in **Figure 2(b)** against the dimensionless characteristic length for different values of the mixture parameter ($\alpha = 0.0,\ 0.2, 0.4, 0.6, 0.8$ and 1.0).

As can be observed, the normalised CMOD, δ^*, decreases by increasing the value of λ for all the considered values of the mixture parameter, with the exception of $\alpha = 1.0$ (thick line), for which $\delta^* = 1.0$ being such a case corresponding to the local Bernoulli-Euler problem.

Moreover, for λ tending to zero, that is, when l? L_c, the nanobeam behaves as an edge-cracked beam with large-scale sizes. On the contrary, for λ greater than 0.0, the normalised CMOD significantly decreases and the decrement is maximum (of about 70%) when $\lambda = 1.0$ and $\alpha = 0.0$ (thin continuous line), which corresponds to the fully nonlocal model with the limit condition of $l = L_c$. Consequently, in an ECN, the crack is less open than in a large-scale edge-cracked beam. Finally, by increasing α from 0.0 to 1.0, δ^* progressively increases up to the limit value equal to 1.0 (pure local problem).

2.2 Energy Release Rate and Stress Intensity Factor

In order to determine the Energy release rate per unit width(or crack extension force), ERR, by taking full advantage from the Castigliano Theorem, the total strain energy stored in the deformed ECN is computed as the work done by the two external forces, F, as:

$$W = 2\left[\frac{1}{2}Fv(l)\right] = \frac{F^2 l^3}{3IE} - (\alpha - 1)\frac{F^2 L_c}{IE}\left\{L_c^2\left(1 - e^{-(l/L_c)}\right) - L_c l e^{-(l/L_c)} - \frac{1}{2}l^2\right\} \quad (5)$$

Then, according to the classical linear elastic fracture mechanics, the ERR is given by:

$$G = \frac{1}{b}\frac{dW}{dl} = \frac{F^2 l^2}{bIE}\left\{1 - \lambda(\alpha - 1)\left(e^{-(1/\lambda)} - 1\right)\right\} \quad (6)$$

The above energy release rate may be more conveniently normalised with respect to the well-known classical local Bernoulli-Euler solution, G_C, as:

$$G^* = \frac{G}{G_C} = 1 - \lambda(\alpha - 1)\left(e^{-(1/\lambda)} - 1\right) \quad (7)$$

where

$$G_C = \frac{F^2 l^2}{bEI} \quad (8)$$

the ERR related to a macro-scale double-cantilever beam (i.e. $\lambda = 0.0$ or $\alpha = 1.0$).

The normalised ERR of **Eq.(7)** is then plotted in **Figure 3(a)** against the dimensionless characteristic length, λ, for six values of α.

It is interesting to note that the normalised ERR, G^*, always decreases by increasing λ for all the considered values of the mixture parameter, with the exception of $\alpha = 1.0$ (thick line), for which $G^* = 1.0$ (that is, the local Bernoulli-Euler problem). Moreover, for α equal to 0.0 (thin continuous line), up to a value of the dimensionless characteristic length equal to about 0.5, the decreasing is quick (of about 43%), whereas for λ moving from 0.5

to 1.0, the decreasing is slightly slower (of about 20%). In addition, by increasing α from 0.0 to 1.0, the normalised ERR progressively increases up to the limit value equal to 1.0 (pure local problem). From the above comments, it is possible to conclude that, in an ECN ($\lambda \neq 0.0$ and $\alpha \neq 1.0$), the energy delivered by the system for an additional crack of size dl is lower than that for a crack in a large-scale edge-cracked beam ($\lambda = 0.0$ or $\alpha = 1.0$). Moreover, it can be stated that in an ECN the crack growth depends not only on the crack length (like in a large-scale cracked beam) but also on the characteristic length, L_c, since, according to the linear fracture mechanics concepts, the increment dl of the crack is possible when the delivered energy is equal or greater that the energy required to form an additional crack.

Finally, the Stress Intensity Factor (SIF) for ECN can be computed by taking advantage of the well-known relationship between ERR and SIF that, under plane stress assumption, is given by:

$$K = \sqrt{EG} = Fl\sqrt{\frac{1}{bI}\left\{1-\lambda(\alpha-1)\left(e^{-(1/\lambda)}-1\right)\right\}} \tag{9}$$

where E is the elastic modulus of the material.

The above SIF may be conveniently normalised with respect to the well-known classical local Bernoulli-Euler solution, K_C, as:

$$K^* = \frac{K}{K_C} = \sqrt{1-\lambda(\alpha-1)\left(e^{-(1/\lambda)}-1\right)} \tag{10}$$

where

$$K_C = Fl\sqrt{\frac{1}{bI}} \tag{11}$$

the SIF related to macro-scale double-cantilever beam ($\lambda = 0.0$ or $\alpha = 1.0$).

In **Figure 3(b)**, the normalised SIF is plotted against λ for different values of α. Comments, similar to the above ones for the ERR, may be done also for K^*. In such a case, the maximum decreasing of the normalised SIF is of about 40% when $\alpha = 0.0$ and λ tends to 1.0 (thin continuous line).

3. FRACTURE ANALYSIS OF A CENTRALLY-CRACKED NANOBEAM

3.1 Transversal displacement and CMOD

In the present Section, the fracture behaviour of an Centrally-Cracked Nanobeam (CCN), containing a central crack with a length l (**Figure 4(a)**), and subjected to a pair of concentrated forces at the half crack length, is analysed. The presence of the crack may be conveniently modelled by assuming it as a pair of double-clamped nanobeams having length equal to l, as shown in **Figure 4(b) [55]**.

The CCN has a rectangular cross-section with thickness, $2h$, and width, b. The deformed crack faces of the pair of double-clamped nanobeams under the action of the external loads may be analysed by computing the deflection of the two identical clamped-clamped nanobeams. By taking advantage of the above symmetry, a single double-clamped nanobeam is considered (i.e. the upper one in **Figure 4(b)**) and the transversal displacement may be described by the functions $v_1(x)$, for $0 \le x \le l/2$, and $v_2(x)$, for $l/2 \le x \le l$, under Bernoulli-Euler assumption (see **Figure 4(b)**).

Due to the internal discontinuity caused by the external force, F, in correspondence of $x = l/2$, the displacement equations shall be written in order to take into account the effect of the discontinuity on the nanobeam nonlocal behaviour. Caporale et al. **[53]** developed a new formulation of the fully nonlocal SDM accounting for such an internal discontinuity.

In the present work, the above formulation has been extended in order to include the mixture parameter and to propose a new two-

phase local/nonlocal SDM formulation suitable for nanobeams problems involving internal discontinuity.

A detailed description of the proposed formulation, employed in the following, may be found in **Appendix A.2.**

The displacement functions $v_1(x)$ and $v_2(x)$ can be determined by solving the following sixth-order differential equations:

$$v_1^{(6)}(x) - \frac{1}{L_c^2} v_1^{(4)}(x) = 0 \quad \text{for} \quad 0 \le x \le l/2 \tag{12a}$$

$$v_2^{(6)}(x) - \frac{1}{L_c^2} v_2^{(4)}(x) = 0 \quad \text{for} \quad l/2 \le x \le l \tag{12b}$$

and by imposing the non-homogeneous system represented by the following twelve boundary conditions:

(i) two Constitutive Boundary Conditions (CBCs):

$$v_1^{(3)}(0) - \frac{1}{L_c} v_1^{(2)}(0) = \alpha \frac{M_1^{(1)}(0)}{IE} - \frac{\alpha}{L_c} \frac{M_1(0)}{IE} \tag{13a}$$

$$v_2^{(3)}(l) + \frac{1}{L_c} v_2^{(2)}(l) = \alpha \frac{M_2^{(1)}(l)}{IE} + \frac{\alpha}{L_c} \frac{M_2(l)}{IE} \tag{13b}$$

where M_1 and M_2 are the bending moments acting on the left ($0 \le x \le l/2$) and right ($l/2 \le x \le l$) parts of the nanobeam, respectively;

(ii) two proposed Constitutive Continuity Conditions (CCCs):

$$v_1^{(3)}(l/2) + \frac{1}{L_c} v_1^{(2)}(l/2) = \alpha \frac{M_2^{(1)}(l/2)}{IE} + \frac{\alpha}{L_c} \frac{M_1(l/2)}{IE} + \frac{2(1-\alpha)}{L_c} \chi_{1,2}(l/2) \tag{14a}$$

$$v_2^{(3)}(l/2) - \frac{1}{L_c} v_2^{(2)}(l/2) = \alpha \frac{M_2^{(1)}(l/2)}{IE} - \frac{\alpha}{L_c} \frac{M_2(l/2)}{IE} - \frac{2(1-\alpha)}{L_c} \chi_{2,1}(l/2) \tag{14b}$$

where $\chi_{1,2}(l/2)$ and $\chi_{2,1}(l/2)$ are defined in **Appendix A.2;**

(iii) six Kinematic Boundary Conditions (KBCs):

$$v_1(0) = 0 \tag{15a}$$

$$v_1^{(1)}(0) = 0 \tag{15b}$$

$$v_2(l)=0 \tag{15c}$$

$$v_2^{(1)}(l)=0 \tag{15d}$$

$$v_1(l/2)=v_2(l/2) \tag{15e}$$

$$v_1^{(1)}(l/2)=v_2^{(1)}(l/2) \tag{15f}$$

(iv) and two Static Boundary Conditions (SBCs):

$$v_1^{(3)}(l/2)-L_c^2 v_1^{(5)}(l/2)+\frac{F}{IE}=v_2^{(3)}(l/2)-L_c^2 v_2^{(5)}(l/2) \tag{16a}$$

$$v_1^{(2)}(l/2)-L_c^2 v_1^{(4)}(l/2)=v_2^{(2)}(l/2)-L_c^2 v_2^{(4)}(l/2) \tag{16b}$$

Since the two transversal displacement functions $v_1(x)$ and $v_2(x)$, obtained by solving the above system, are extremely long and complex, their equations are not reported in the present work for sake of brevity.

The maximum deflection is attained at the nanobeam half length (that is, for $x=l/2$), where $v_1(l/2)=v_2(l/2)$.

The transversal displacement normalised with respect to the maximum deflection according to the classical local Bernoulli-Euler solution, that is, $v_1^*(x)=v_1(x)\Big/\left(Fl^3/192EI\right)$ and $v_2^*(x)=v_2(x)\Big/\left(Fl^3/192EI\right)$, is plotted in **Figure 5(a)** against the dimensionless abscissa x/l for different values of α and $\lambda=0.1$.

Figure 5

It is interesting to note the dependency of the normalised transversal displacement on the mixture parameter, α. The case with $\alpha=1.0$ (thick line) corresponds to the case of the classical Bernoulli-Euler local problem. For smaller value of α, the normalised displacement values are lower showing a decrement of about 41% for $\alpha=0.0$ (fully nonlocal model) and $x/l=0.5$ (that is, at the half

length). Consequently, the nanobeam shows a stiffer behaviour with respect to a large-scale beam.

The maximum Crack Opening Displacement (COD), δ, may be computed as two-times the deflection at the half length of the double-clamped nanobeam, that is, $\delta = 2 \cdot v_1(l/2) = 2 \cdot v_2(l/2)$. Therefore, such a COD may be conveniently normalised with respect to the well-known classical local Bernoulli-Euler solution, δ_C, as:

$$\delta^* = \frac{\delta}{\delta_C} \tag{17}$$

with

$$\delta_C = 2 \cdot \frac{Fl^3}{192IE} \tag{18}$$

The normalised COD is then plotted in **Figure 5(b)** against the dimensionless characteristic length for different values of the mixture parameter α.

As can be observed, the normalised COD, δ^*, decreases by increasing the value of λ for all the considered values of the mixture parameter, with the exception of $\alpha = 1.0$ (thick line), for which $\delta^* = 1.0$ (local Bernoulli-Euler problem). The decrement is maximum (of about 95%) when $\lambda = 1.0$ and $\alpha = 0.0$ (thin continuous line), which corresponds to the fully nonlocal model. Consequently, it is possible to state that in a CCN the crack is less open than in a large-scale centrally-cracked beam.

Finally, by increasing α from 0.0 to 1.0, δ^* progressively increases up to the limit value equal to 1.0 (pure local problem).

3.2 Energy Release Rate and Stress Intensity Factor

In order to determine the Energy release rate per unit width (or crack extension force), ERR, the same procedure presented in **Section**

2.2 is employed. The total strain energy stored in the deformed CCN is computed as the work done by the two external forces, F:

$$W = 2\left[\frac{1}{2}Fv_1(l)\right] = 2\left[\frac{1}{2}Fv_2(l)\right] \tag{19}$$

and the ERR is given by:

$$G = \frac{1}{b}\frac{dW}{dl} \tag{20}$$

The above energy release rate is then normalised with respect to the classical local solution, G_C, as:

$$G^* = \frac{G}{G_C} \tag{21}$$

where

$$G_C = \frac{F^2 l^2}{64bEI} \tag{22}$$

the ERR related to the double-cantilever beam ($\lambda = 0.0$ or $\alpha = 1.0$).

The normalised ERR is then plotted in **Figure 6(a)** against the dimensionless characteristic length, λ, for different values of α.

From **Figure 6(a)**, it is possible to observe that the normalised ERR, G^*, always decreases by increasing λ for all the considered values of the mixture parameter, with the exception of $\alpha = 1.0$ (thick line), for which $G^* = 1.0$ (i.e. local Bernoulli-Euler problem). Moreover, for α equal to 0.0 (thin continuous line), up to a value of the dimensionless characteristic length equal to about 0.3, the decreasing is quick (of about 74%), whereas for λ moving from 0.3 to 1.0, the decreasing is slower (of about 20%). In addition, by

increasing α from 0.0 to 1.0, the normalised ERR progressively increases up to the limit value equal to 1.0 (pure local problem). From the above comments, it is possible to conclude that, also in a CCN ($\lambda \neq 0.0$ and $\alpha \neq 1.0$), the energy delivered by the system for an additional crack of size dl is lower than that corresponding to a crack in a large-scale centrally-cracked beam ($\lambda = 0.0$ or $\alpha = 1.0$). Moreover, it can be stated that in a CCN the crack growth depends not only on the crack length (like in a large-scale cracked beam), but also on the material characteristic length, L_c.

Finally, the Stress Intensity Factor (SIF) for CCN is computed by taking advantage of the well-known relationship between ERR and SIF under plane stress assumption:

$$K = \sqrt{EG} \tag{23}$$

where E is the elastic modulus of the material.

The above SIF may be conveniently normalised with respect to the well-known classical local Bernoulli-Euler solution, K_C, as:

$$K^* = \frac{K}{K_C} \tag{24}$$

where

$$K_C = \frac{Fl}{8}\sqrt{\frac{1}{bI}} \tag{25}$$

the SIF related to the double-cantilever beam ($\lambda = 0.0$ or $\alpha = 1.0$).

In **Figure 6(b)**, the normalised SIF is plotted against λ for different values of α. Similar comments may be done for K^* and the maximum decrement (of 80%) is observed when $\alpha = 0.0$ and λ tends to 1.0 (thin continuous line).

3. STRESS FIELD AHEAD THE CRACK TIP

The stress field ahead the crack tip is computed by employing the approximated solution proposed by Yuanhan **[58]**. The Author presented a solution for the Griffith crack problem based on the nonlocal elasticity and the approximate stress formulae of the classical fracture mechanics. More precisely, the Author defined the one-dimensional stress field in four regions depending on the crack length and the material characteristic length **[58]**.

By taking the polar coordinates (r,θ), with its origin at the crack tip and the x'-axis, with its origin in O' as shown in **Figure 7(a)**, a normalised one-dimensional stress, σ_y^*, (with $\theta = 0°$) is computed as the ratio between the stress, σ_y, according to Refs **[55, 58]**, and $\sigma_{y,max}$, that is:

$$\sigma_y^* = \frac{\sigma_y}{\sigma_{y,\max}} = 0 \qquad 0 \le x' < l - L_c \qquad (26a)$$

$$\sigma_y^* = \frac{\sigma_y}{\sigma_{y,\max}} \cong 0.866 \cdot \left(1 + \frac{x'-l}{L_c}\right)^{\frac{3}{2}} \qquad l - L_c \le x' < l \qquad (26b)$$

$$\sigma_y^* = \frac{\sigma_y}{\sigma_{y,\max}} \cong 0.866 \cdot \left[\left(1 + \frac{x'-l}{L_c}\right)^{\frac{3}{2}} - 2\left(\frac{x'-l}{L_c}\right)^{\frac{3}{2}}\right] \qquad l \le x' < l + L_c \qquad (26c)$$

$$\sigma_y^* = \frac{\sigma_y}{\sigma_{y,\max}} \cong 0.866 \cdot \left[\left(1 + \frac{x'-l}{L_c}\right)^{\frac{3}{2}} - 2\left(\frac{x'-l}{L_c}\right)^{\frac{3}{2}} + \left(-1 + \frac{x'-l}{L_c}\right)^{\frac{3}{2}}\right] \qquad x' \ge l + L_c \qquad (26d)$$

where

$$\sigma_{y,max} \cong 1.155 \cdot \frac{4}{3} \frac{K}{\sqrt{2\pi L_c}} \qquad (27)$$

attained in correspondence of $x' = l + L_c / 3$.

Note that, such a solution assumes that σ_y is invariable between two adjacent atoms along y-axis, and gives a good accuracy of the exact one, provided by Eringen **[59]**, for λ greater than about 0.05, as it was proved in Ref. **[58]**.

In **Figure 7(b)**, the normalised one-dimensional stress field (for $\theta = 0°$) is plotted against the dimensionless radial coordinate, $r^* = r/l$ for different values of λ. It can be observed that the stress at the crack tip (that is, $r^* = 0.0$ in **Figure 7(b)**), calculated by using the nonlocal elasticity theory, is a finite value (about 0.87) for all the examined values of the dimensionless characteristic length, contrary to the result obtained by employing the classical fracture mechanics (for which the stress tends to infinity). Note that the one-dimensional stress field here plotted is the same for both edge- and centrally-cracked nanobeams, and that the mixture parameter has not been implemented in the above formulation (this is equivalent to assume $\alpha = 0.0$, that is, pure nonlocal model).

4. COMPARISON WITH LITERATURE RESULTS

Finally, in the present Section, the two cracked nanobeams are analysed by means of the Gradient Elasticity Theory based model proposed by Zhang et al. in Ref. **[54]**. The Authors presented the formulation for calculating the Energy Release Rate and the Stress Intensity Factor for both edge- and centrally-cracked nanobeams; formulation which has been here employed to make a comparison with the results obtained by applying the local/nonlocal SDM. In the following, only the results computed through the Gradient Elasticity Theory (named, for simplicity, Grad-Ela) are reported, whereas details about the solutions may be found in Ref. **[54]**.

According to the above Grad-Ela model, two material characteristic lengths, l_1 and l_2, are introduced and the fracture properties are defined as function also of the ratio l/h, depending on the geometry of the cracked nanobeam. The Authors assumed the two characteristic

lengths, l_1 and l_2, equal to a unique value, $\bar{l}$, that, in accordance to the symbols used in the present paper, it can be taken equal to L_c (i.e. $\bar{l} = L_c$). On the contrary, since the two-phase local/nonlocal SDM is independent of l/h, in order to obtain comparable results, such a ratio has been taken equal to three values, that is, $l/h = 0.1, 0.5, 1.0$.

In **Figure 8**, the Energy Release Rate values, normalised with respect to the classical solutions (see **Sections 2** and **3**), are plotted against the dimensionless characteristic length, λ, by considering the above three values of l/h and three values of the mixture parameter α. In particular, in **Figure 8(a)**, the results related the ECN are reported, whereas those related to the CCN are represented in the **Figure 8(b)**. It can be observed that, the normalised ERR of the ECN (**Fig. 8(a)**) computed through the Grad-Ela assumes values lower that those determined by employing the SDM also for different values of α. On the contrary, for the CCN (**Fig. 8(b)**), a certain similarity may be observed especially by varying the mixture parameter from 0.0 to 0.4. Consequently, in the case of a central crack, the two models are able to give comparable results if the geometry and mixture parameters are properly set, while, in the case of an edge crack, the outcome results are quite different independent of the set parameters.

The same trends are also observed for the normalised Stress Intensity Factor plotted in **Figure 9** for both cracked nanobeams.

5. CONCLUSIONS

In the present paper, the two-phase local/nonlocal stress-driven integral model has been employed, together with the Bernoulli-Euler beam theory, to analysed size-dependent Mode I fracture behaviour of both edge- and centrally-cracked nanobeams.

For the two nanobeams configurations, the transversal displacements and the crack opening displacements have been computed by varying both dimensionless characteristic length and mixture

parameter values. The energy release rate, the stress intensity factor, and the stress field near the crack tip have been determined by employing the compliance method and the linear elastic fracture mechanics concepts. From the obtained results, it has been observed that the analysed fracture properties vary significantly with the dimensionless characteristic length of the material, manifesting the so-called small-scale effect. In particular, the energy release rate strongly decreases by increasing the nonlocality, showing a less stiff behaviour of the cracked nanobeams with respect to the large-scale cracked beam. As a consequence, the fracture performance of nanobeams appears superior with respect to large-scale beams.

Finally, a comparison with literature results has been made. Also applying the gradient elastic theory, the scale-effect is appreciable and the better fracture performance of nanobeams with respect to large-scale beams is observed, even if in a quantitative different way with respect to that noticed by employing the two-phase local/nonlocal SDM (especially in the case of the edge-cracked nanobeam).

Data availability

The raw data required to reproduce these findings cannot be shared at this time as the data also forms part of an ongoing study.

REFERENCES

[1] Belytschko T, Xiao SP, Schatz GC, Ruoff RS. Atomistic simulations of nanotube fracture. Physical Review B 2002;65(23):art.235430.
[2] Huang S, Zhang S, Belytschko T, Terdalkar SS, Zhu T. Mechanics of nanocrack: Fracture, dislocation emission, and amorphization. Journal of the Mechanics and Physics of Solids 2009;57(5):840-850.
[3] Barretta R, Luciano R, Marotti De Sciarra F. A fully gradient model for euler-bernoulli nanobeams. Mathematical Problems in Engineering 2015;art.495095.
[4] Zhao P, Zhang K, Deng Z. Size effects on the band gap of flexural wave propagation in one-dimensional periodic micro-beams. Composite Structures 2021;271:art.114162.
[5] Phung-Van P, Ferreira AJM, Nguyen-Xuan H, Thai CH. Scale-dependent nonlocal strain gradient isogeometric analysis of metal foam nanoscale plates with various porosity distributions. Composite Structures 2021;268:art.113949.
[6] Fang TH, Li WL, Tao NR, Lu K. Revealing Extraordinary Intrinsic Tensile Plasticity in Gradient Nano-Grained Copper. Science 2011;331:1587-1590.
[7] Wu XL, Jiang P, Chena L, Yuan F, Zhu YT. Extraordinary strain hardening by gradient structure. PNAS 2014;111:7197-7201.
[8] Peng C, Zhan Y, Lou J. Size-dependent fracture mode transition in copper nanowires. Small 2012;8(12):1889-1894.
[9] Le MQ, Batra RC. Single-edge crack growth in graphene sheets under tension. Computational Materials Science 2013;69:381-388.
[10] Cheng SH, Sun CT. Size-dependent fracture toughness of nanoscale structures: Crack-tip stress approach in molecular dynamics. Journal of Nanomechanics and Micromechanics 2014;4(4):art.A4014001.
[11] Li XF, Wang BL. Bending and fracture properties of small scale elastic beams - A nonlocal analysis. Applied Mechanics and Materials 2012;152-154:1417-1426.
[12] Yan Z, Jiang L. Size-dependent bending and vibration behaviour of piezoelectric nanobeams due to flexoelectricity. Journal of Physics D: Applied Physics 2013;46:art.355502.
[13] Yang Y. Bending analysis of carbon nanotubes based on analytical nonlocal timoshenko beam model. Applied Mechanics and Materials 2014;444-445:202-208.
[14] Li YS, Ma P, Wang W. Bending, buckling, and free vibration of magnetoelectroelastic nanobeam based on nonlocal theory. Journal of Intelligent Material Systems and Structures 2016;27:1139-1149.
[15] Karami B, Janghorban M, Rabczuk T. Static analysis of functionally graded anisotropic nanoplates using nonlocal strain gradient theory. Composite Structures 2019;227:art.111249.
[16] Daikh AA, Houari MSA, Eltaher MA. A novel nonlocal strain gradient Quasi-3D bending analysis of sigmoid functionally graded sandwich nanoplates. Composite Structures 2021;262:art.113347.
[17] Zhang P, Qing H. Closed-form solution in bi-Helmholtz kernel based two-phase nonlocal integral models for functionally graded Timoshenko beams. Composite Structures 2021;265:art.113770.
[18] Dastjerdi S, Malikan M, Dimitri R, Tornabene F. Nonlocal elasticity analysis of moderately thick porous functionally graded plates in a hygro-thermal environment. Composite Structures 2021;255:art.112925.
[19] Yang Y, Lim CW. Non-classical stiffness strengthening size effects for free vibration of a nonlocal nanostructure. International Journal of Mechanical Sciences 2012;54:57-68.
[20] Eptaimeros KG, Koutsoumaris CC, Tsamasphyros GJ. Nonlocal integral approach to the dynamical response of nanobeams. International Journal of Mechanical Sciences 2016;115-116:68-80.
[21] Hoang VNV, Minh VT, Ninh DG, Nguyen CT, Huy VL. Effects of non-uniform elastic foundation on the nonlinear vibration of nanocomposite plates in thermal environment using Selvadurai methodology. Composite Structures 2020;253:art.112812.
[22] Cao Y, Khorami M, Baharom S, Assilzadeh H, Hassan Dindarloo M. The effects of multi-directional functionally graded materials on the natural frequency of the doubly-curved nanoshells. Composite Structures 2021;258:art.113403.
[23] Penna R, Feo L, Fortunato A, Luciano R. Nonlinear free vibrations analysis

of geometrically imperfect FG nano-beams based on stress-driven nonlocal elasticity with initial pretension force. Composite Structures 2021;255:art.112856.
[24] Kiani K, Żur KK. Vibrations of double-nanorod-systems with defects using nonlocal-integral-surface energy-based formulations. Composite Structures 2021;256:art.113028.
[25] Lu L, Wang S, Li M, Guo X. Free vibration and dynamic stability of functionally graded composite microtubes reinforced with graphene platelets. Composite Structures 2021;272:art.114231.
[26] Cornacchia F, Fabbrocino F, Fantuzzi N, Luciano R, Penna R. Analytical solution of cross- and angle-ply nano plates with strain gradient theory for linear vibrations and buckling. Mechanics of Advanced Materials and Structures 2021;8(12):1201-1215.
[27] Tocci Monaco G, Fantuzzi N, Fabbrocino F, Luciano R. Hygro-thermal vibrations and buckling of laminated nanoplates via nonlocal strain gradient theory. Composite Structures 2021;262:art.113337.
[28] Tong LH, Lin F, Xiang Y, Shen HS, Lim CW. Buckling analysis of nanoplates based on a generic third-order plate theory with shear-dependent non-isotropic surface stresses. Composite Structures 2021;265:art.113708.
[29] Wang H, Li X, Tang G, Shen Z. Effect of Surface Stress on Stress Intensity Factors of a Nanoscale Crack via Double Cantilever Beam Model. Journal of Nanoscience and Nanotechnology 2013;13:477–482.
[30] Luo SS, You ZS, Lu L. Intrinsic fracture toughness of bulk nanostructured Cu with nanoscale deformation twins. Scripta Materialia 2017;133:1-4.
[31] Zha X, Jiang F, Xu X. Investigation of modelling and stress distribution of a coating/substrate system after an indentation test. International Journal of Mechanical Sciences 2017;134:1-14.
[32] Gangele A, Pandey AK. Elastic and fracture characteristics of graphene-silicon nanosheet composites using nonlinear finite element method. International Journal of Mechanical Sciences 2018;142-143:491-501.
[33] Deng J, Liao N, Zhang M, Xue W. Extended finite element analysis of plastic and fracture behaviors of SiC-based multi-layer thin films system. International Journal of Mechanical Sciences 2019;161-162:art.105017.
[34] Romano G, Barretta R. Stress-driven versus strain-driven nonlocal integral model for elastic nano-beams. Composites Part B: Engineering 2017;114:184-188.
[35] Romano G, Barretta R. Nonlocal elasticity in nanobeams: the stress-driven integral model. International Journal of Engineering Science 2017;115:14-27.
[36] Apuzzo A, Barretta R, Luciano R, Marotti de Sciarra F, Penna R. Free vibrations of Bernoulli-Euler nano-beams by the stress-driven nonlocal integral model. Composites Part B: Engineering 2017;123,105-111.
[37] Barretta R, Fazelzadeh SA, Feo L, Ghavanloo E, Luciano, R. Nonlocal inflected nano-beams: A stress-driven approach of bi-Helmholtz type. Composite Structures 2018;200:239-245.
[38] Darban H, Fabbrocino F, Feo L, Luciano R. Size-dependent buckling analysis of nanobeams resting on two-parameter elastic foundation through stress-driven nonlocal elasticity model. Mechanics of Advanced Materials and Structures 2020, in press, doi: 10.1080/15376494.2020.1739357.
[39] Darban H, Luciano R, Caporale A, Fabbrocino F. Higher modes of buckling in shear deformable nanobeams. International Journal of Engineering Science 2020;154,art.103338.
[40] Luciano R, Caporale A, Darban H, Bartolomeo C. Variational approaches for bending and buckling of non-local stress-driven Timoshenko nano-beams for smart materials. Mechanics Research Communications 2020;103:art.103470.
[41] Luciano R, Darban H, Bartolomeo C, Fabbrocino F, Scorza D. Free flexural vibrations of nanobeams with non-classical boundary conditions using stress-driven nonlocal model. Mechanics Research Communications 2020:107;art.103536.
[42] Eringen AC. Nonlocal polar elastic continua. International Journal of Engineering Science 1972;10:1-16.
[43] Eringen AC, Edelen DGB. On nonlocal elasticity. International Journal of Engineering Science 1972;10:233-248.
[44] Peddieson J, Buchanan GR, McNitt RP. Application of nonlocal continuum models to nanotechnology. International Journal of Engineering Science 2003;41:305–312.

[45] Romano G, Barretta R, Diaco M, Marotti de Sciarra F. Constitutive boundary conditions and paradoxes in nonlocal elastic nano-beams. International Journal of Mechanical Science 2017;121:151–156.
[46] Apuzzo A, Barretta R, Fabbrocino F, Faghidian SA, Luciano R, Marotta De Sciarra F. Axial and torsional free vibrations of elastic nano-beams by stress-driven two-phase elasticity. Journal of Applied and Computational Mechanics 2019;5(2):402-413.
[47] Barretta R, Diaco M, Feo L, Luciano R, Marotti De Sciarra F, Penna R. Stress-driven integral elastic theory for torsion of nano-beams. Mechanics Research Communications 2018;87:35-41.
[48] Barretta R, Fabbrocino F, Luciano R, Marotti De Sciarra F, Ruta G. Buckling loads of nano-beams in stress-driven nonlocal elasticity. Mechanics of Advanced Materials and Structures 2020;27(11):869-875.
[49] Barretta R, Faghidian SA, Luciano R. Longitudinal vibrations of nano-rods by stress-driven integral elasticity Mechanics of Advanced Materials and Structures 2020;26(15):1307-1315.
[50] Romano G, Barretta R, Diaco M. On nonlocal integral models for elastic nano-beams. International Journal of Mechanical Sciences 2017;131-132:490-499.
[51] Barretta R, Fabbrocino F, Luciano R, De Sciarra FM. Closed-form solutions in stress-driven two-phase integral elasticity for bending of functionally graded nano-beams. Physica E 2018;97:13–30.
[52] Apuzzo A, Bartolomeo C, Luciano R, Scorza D. Novel local/nonlocal formulation of the stress-driven model through closed form solution for higher vibrations modes. Composite Structures 2020;252:art.112688.
[53] Caporale A, Darban H, Luciano R. Exact closed-form solutions for nonlocal beams with loading discontinuities. Mechanics of Advanced Materials and Structures 2020:1-11.
[54] Zhang H, Li XF, Tang GJ, Shen ZB. Stress intensity factors of double cantilever nanobeams via gradient elasticity theory. Engineering Fracture Mechanics 2013;105:58-64.
[55] Vantadori S, Luciano R, Scorza D, Darban H. Fracture analysis of nanobeams based on the stress-driven non-local theory of elasticity. Mechanics of Advanced Materials and Structures 2020, article in press. doi:10.1080/15376494.2020.1846231.
[56] Li S, Wang J, Thouless MD. The effects of shear on delamination in layered materials. Journal of the Mechanics and Physics of Solids 2004:52;193-214.
[57] Thouless MD. Shear forces, root rotations, phase angles and delamination of layered materials. Engineering Fracture Mechanics 2018;191:153-167.
[58] Yuanhan W. Approximate stress analysis near crack tip by non-local elasticity. International Journal of Fracture 1992;53:21-32.
[59] Eringen AC, Speziale CG, Kim BS. Crack-tip problem in non-local elasticity. Journal of the Mechanics and Physics of Solids 1977;25:339-355.

APPENDIX

A.1 Local/nonlocal SDM formualtion for a cantilever nanobeam

Let us consider a flexible nanobeam with the longitudinal coordinate as x, and the through the thickness coordinate, perpendicular to the neutral axis of the non-deformed nanobeam, as y (**Figure A.1**).

Figure A.1

Under the Bernoulli-Euler assumption, the flexural curvature field, $\chi(x)$, is expressed as:

$$\chi(x) = v^{(2)}(x) \tag{A.1}$$

where $v(x)$ is the transverse displacement, and $(\mathrm{K})^{(n)}$ stays for the n^{th}-order derivative with respect to x.

According to the local/nonlocal SDM **[51]**, $\chi(x)$ can be computed through the integral convolution, as here reported:

$$\chi(x) = \alpha \frac{M(x)}{I_E} + (1-\alpha) \int_0^l \psi(x-t, L_c) \frac{M(t)}{IE} dt \tag{A.2}$$

where t is the integration variable, α is the mixture parameter, and IE is the local elastic stiffness:

$$IE = \int_{\Omega} Ey^2 dA \tag{A.3}$$

being Ω the area of the nanobeam cross-section.

Moreover, ψ is the special kernel, defined as:

$$\psi\left(x, L_c\right) = \frac{1}{2L_c} exp\left(-\frac{|x|}{L_c}\right) \qquad \textbf{(A.4)}$$

where the nanobeam characteristic length, L_c, is defined as the product of a dimensionless nonlocal parameter, λ, and the nanobeam length, l (that is, $L_c = \lambda\, l$).

Eq. (A.2) is equivalent to the following second order differential equation:

$$\chi^{(2)}(x) - \frac{1}{L_c^2}\chi\,(x) = \alpha\frac{M^{(2)}(x)}{IE} - \frac{1}{L_c^2}\frac{M\,(x)}{IE} \qquad \textbf{(A.5)}$$

together with the following constitutive boundary conditions:

$$\chi^{(1)}(0) - \frac{1}{L_c}\chi(0) = \alpha\frac{M^{(1)}(0)}{IE} - \frac{\alpha}{L_c}\frac{M(0)}{IE} \qquad \textbf{(A.6a)}$$

$$\chi^{(1)}(l) + \frac{1}{L_c}\chi(l) = \alpha\frac{M^{(1)}(l)}{I_E} + \frac{\alpha}{L_c}\frac{M(l)}{I_E} \qquad \textbf{(A.6b)}$$

where M stands for bending moment.

By differentiating **Eq.(A.5)** to times with respect to x, and by exploiting the differential condition of **Eq. (A.1)**, the following equation is obtained:

$$L_c^2 v^{(6)} - v^{(4)} = 0 \qquad \textbf{(A.7)}$$

In such a context, **Eqs (A.6)** can be rewritten, in a more convenient way, in terms of deflection, v:

$$v^{(3)}(0) - \frac{1}{L_c}v^{(2)}(0) = \alpha\frac{M^{(1)}(0)}{IE} - \frac{\alpha}{L_c}\frac{M(0)}{IE} \qquad \textbf{(A.8a)}$$

$$v^{(3)}(l)+\frac{1}{L_c}v^{(2)}(l)=\alpha\frac{M^{(1)}(l)}{IE}+\frac{\alpha}{L_c}\frac{M(l)}{IE} \qquad \textbf{(A.8b)}$$

By solving **Eq. (A.7),** the general integral depends on six integration constants. Therefore, by imposing six boundary conditions that is, the two constitutive boundary conditions represented by **Eqs (A.8)** and four suitable kinematic/static boundary conditions at the nanobeam ends (according to the Bernoulli-Euler theory), a non-homogeneous algebraic system is in general obtained, which equations are expressed in terms of the above six integration constants.

A.2 local/nonlocal SDM formulation for a flexible nanobeam with internal discontinuies

The formulation of the ~~full~~ fully nonlocal stress-driven model for nanobeams with internal discontinuities is here extended in order to introduce the mixture parameter, α, able to proper combine the local/nonlocal phases of the model.

Let us consider the nanobeam as a straight beam with loading discontinuities at abscissa $x=x_d$ as shown in **Figure A.2.**

Figure A.2

The curvature $\chi(x)$ at a generic point x is defined as the following integral convolution **[51]:**

$$\chi(x)=\alpha\frac{M(x)}{IE}+(1-\alpha)\int_0^l \psi(x-t,L_c)\frac{M(t)}{IE}dt \qquad (A.9)$$

where $M(x)$ and I_E are bending moment and bending stiffness, respectively; $\psi(x-t,L_c)$ is an averaging kernel depending on the small scale parameter L_c and α is the mixture parameter. Taking into

account the presence of force and couple concentrated at a generic point with abscissa x_d ($0 < x_d < l$), the integral at the right-hand side of **Eq.(A.9)** is written as:

$$\chi(x) = \alpha \frac{M_1(x)}{IE} + (1-\alpha) \int_0^{x_d} \psi(x-t, L_c) \frac{M_1(t)}{IE} dt + \\ + \alpha \frac{M_2(x)}{IE} + (1-\alpha) \int_{x_d}^{l} \psi(x-t, L_c) \frac{M_2(t)}{IE} dt \tag{A.10}$$

where $M_1(x)$ and $M_2(x)$ are the bending moments at the left (namely, first part of the beam) and at the right of a given abscissa x_d (namely, second part of the beam), respectively.

The integral **Eq. (A.10)** is completed with variationally consistent essential and natural boundary and continuity conditions at points with $x = 0, x_d, l$, which are the same as those conditions imposed in local problems.

Assuming the following exponential kernel of **Eq. (A.4)**, it is shown that the integral formulation defined by Eq. **(A.10)** is equivalent to a differential formulation given by two differential equations subject to conventional constitutive boundary conditions of the local/nonlocal SDM and novel constitutive continuity conditions.

The curvature at any point belonging to the first part of nanobeam can be written as:

$$\chi_1(x) = \alpha \frac{M_1(x)}{IE} + (1-\alpha)\left[\chi_{1,l}(x) + \chi_{1,r}(x) + \chi_{1,2}(x)\right] \quad \text{with} \quad x \in [0, x_d[\tag{A.11}$$

where

$$\chi_{1,l}(x) = \int_0^{x} \exp\left[\frac{(t-x)}{L_c}\right] \frac{1}{2L_c} \frac{M_1(t)}{IE} dt \tag{A.12}$$

$$\chi_{1,r}(x)=\int_{x}^{x_d}\exp\left[\frac{(x-t)}{L_c}\right]\frac{1}{2L_c}\frac{M_1(t)}{IE}dt$$

$$\chi_{1,2}(x)=\int_{x_d}^{l}\exp\left[\frac{(x-t)}{L_c}\right]\frac{1}{2L_c}\frac{M_2(t)}{IE}dt$$

The first derivative of the curvature $\chi_1(x)$ can be written as:

$$\begin{aligned}\chi_1^{(1)}(x)&=\alpha\frac{M_1^{(1)}(x)}{IE}+(1-\alpha)\left[\chi_{1,l}^{(1)}(x)+\chi_{1,r}^{(1)}(x)+\chi_{1,2}^{(1)}(x)\right]=\\&=\alpha\frac{M_1^{(1)}(x)}{IE}+(1-\alpha)\left[-\frac{1}{L_c}\chi_{1,l}(x)+\frac{1}{L_c}\chi_{1,r}(x)+\frac{1}{L_c}\chi_{1,2}(x)\right]\end{aligned}\qquad\text{(A.13)}$$

~~being~~ where

$$\begin{aligned}\chi_{1,l}^{(1)}(x)&=\frac{d\chi_{1,l}(x)}{dx}=\frac{1}{L_c}\left[\frac{M_1(x)}{2IE}-\chi_{1,l}(x)\right]\\\chi_{1,r}^{(1)}(x)&=\frac{d\chi_{1,r}(x)}{dx}=\frac{1}{L_c}\left[\chi_{1,r}(x)-\frac{M_1(x)}{2IE}\right]\\\chi_{1,2}^{(1)}(x)&=\frac{d\chi_{1,r}(x)}{dx}=\frac{1}{L_c}\left[\chi_{1,2}(x)\right]\end{aligned}\qquad\text{(A.14)}$$

The second derivative of the curvature $\chi_1(x)$ can be then written as:

$$\begin{aligned}\chi_1^{(2)}(x)&=\alpha\frac{M_1^{(2)}(x)}{IE}+(1-\alpha)\frac{1}{L_c^2}\left[-\frac{M_1(x)}{IE}+\chi_{1,l}(x)+\chi_{1,r}(x)+\chi_{1,2}(x)\right]=\\&=\alpha\frac{M_1^{(2)}(x)}{IE}+\frac{1}{L_c^2}\left\{-\frac{M_1(x)}{IE}+\underbrace{\alpha\frac{M_1(x)}{IE}+(1-\alpha)\left[\chi_{1,l}(x)+\chi_{1,r}(x)+\chi_{1,2}(x)\right]}_{\chi_1(x)}\right\}\end{aligned}\qquad\text{(A.15)}$$

Finally, the differential equation for the first part of beam may be obtained as:

$$\chi_1^{(2)}(x)-\frac{1}{L_c^2}\chi_1(x)=\alpha\frac{M_1^{(2)}(x)}{IE}-\frac{1}{L_c^2}\frac{M_1(x)}{IE}\quad\text{for}\quad x\in[0,x_d[\tag{A.16}$$

Similarly, the differential equation for the second part of the nanobeam is obtained:

$$\chi_2^{(2)}(x)-\frac{1}{L_c^2}\chi_2(x)=\alpha\frac{M_2^{(2)}(x)}{IE}-\frac{1}{L_c^2}\frac{M_2(x)}{IE}\quad\text{for}\quad x\in]x_d,l] \tag{A.17}$$

Eqs (A.16) and **(A.17)** are formally similar to the differential equation of the local/nonlocal formulation without loading discontinuities. On the other hand, continuity conditions in presence of loading discontinuities are not obvious and a proper derivation must be done in order to find a consistent solution.

To this end, **Eq. (A.11)** is first evaluated at boundary and continuity points, that is $x=0,\ x_d$, respectively:

$$\chi_1(0)=\alpha\frac{M_1(0)}{IE}+(1-\alpha)\left[\chi_{1,r}(0)+\chi_{1,2}(0)\right] \tag{A.18a}$$

$$\chi_1(x_d)=\alpha\frac{M_1(x_d)}{IE}+(1-\alpha)\left[\chi_{1,l}(x_d)+\chi_{1,2}(x_d)\right] \tag{A.18b}$$

since $\chi_{1,r}(0)=\chi_{1,l}(x_d)=0$. Then, **Eqs (A.18)** are substituted into **Eq. (A.13)**, evaluated at the same boundary and continuity points, that is, $x=0,\ x_d$:

$$\begin{aligned}
&\chi_1^{(1)}(0)=\alpha\frac{M_1^{(1)}(0)}{IE}+\frac{(1-\alpha)}{L_c}\left[\chi_{1,r}(0)+\chi_{1,2}(0)\right]=\alpha\frac{M_1^{(1)}(0)}{IE}+\frac{1}{L_c}\chi_1(0)-\frac{\alpha}{L_c}\frac{M_1(0)}{IE}\\
&\chi_1^{(1)}(x_d)=\alpha\frac{M_1^{(1)}(x_d)}{IE}+\frac{(1-\alpha)}{L_c}\left[-\chi_{1,l}(x_d)+\chi_{1,2}(x_d)\right]=\\
&\quad=\alpha\frac{M_1^{(1)}(x_d)}{IE}-\frac{1}{L_c}\chi_1(0)+\frac{\alpha}{L_c}\frac{M_1(x_d)}{IE}+\frac{2(1-\alpha)}{L_c}\chi_{1,2}(x_d)
\end{aligned} \tag{A.19}$$

and obtaining the following constitutive boundary and continuity conditions:

$$\chi_1^{(1)}(0)-\frac{1}{L_c}\chi_1(0)=\alpha\frac{M_1^{(1)}(0)}{IE}-\frac{\alpha}{L_c}\frac{M_1(0)}{IE} \tag{A.20a}$$

$$\chi_1^{(1)}(x_d)+\frac{1}{L_c}\chi_1(x_d)=\alpha\frac{M_1^{(1)}(x_d)}{IE}+\frac{\alpha}{L_c}\frac{M_1(x_d)}{IE}+\frac{2(1-\alpha)}{L_c}\chi_{1,2}(x_d) \tag{A.20b}$$

Analogously, the constitutive boundary and continuity conditions for the second part of the beam ($x=x_d,l$) are:

$$\chi_2^{(1)}(x_d)-\frac{1}{L_c}\chi_2(x_d)=\alpha\frac{M_2^{(1)}(x_d)}{IE}-\frac{\alpha}{L_c}\frac{M_2(x_d)}{IE}-\frac{2(1-\alpha)}{L_c}\chi_{2,1}(x_d) \tag{A.21a}$$

$$\chi_2^{(1)}(l)+\frac{1}{L_c}\chi_2(l)=\alpha\frac{M_2^{(1)}(l)}{IE}+\frac{\alpha}{L_c}\frac{M_2(l)}{IE} \tag{A.21b}$$

with

$$\chi_{2,1}(x)=\int_0^{x_d}\exp\left[\frac{(t-x)}{L_c}\right]\frac{1}{2L_c}\frac{M_1(t)}{IE}dt \tag{A.22}$$

The governing equations of the differential problem are given by **Eqs (A.16)** and **(A.17)** subject to the constitutive boundary and continuity conditions of **Eqs (A.20)** and **(A.21)**, which include the integral convolutions $\chi_{1,2}(x)$ and $\chi_{2,1}(x)$, respectively.

Finally, by solving **Eqs (A.16)** and **(A.17)**, the general integral depends on twelve integration constants. Therefore, by imposing twelve boundary conditions that is, the two CBCs plus the new CCCs of **Eqs (A.20)** and **(A.21)**, and eight suitable kinematic/static boundary conditions at the nanobeam ends and at $x=x_d$, a non-homogeneous algebraic system is obtained, which equations are expressed in terms of the above twelve integration constants.

Submitted to **Composite Structures – SI Professor Erasmo Carrera**

August 2021

Version R1, October 2021

FRACTURE BEHAVIOUR OF NANOBEAMS THROUGH TWO-PHASE LOCAL/NONLOCAL STRESS-DRIVEN MODEL

Daniela Scorza[1*], Raimondo Luciano[1], Sabrina Vantadori[2]

[1]Department of Engineering, University of Naples Parthenope, Centro Direzionale Isola C4, 80143 Naples, Italy

[2]Department of Engineering and Architecture – University of Parma Parco Area delle Scienze 181/A, 43124 Parma, Italy

***Corresponding Author:** Daniela Scorza, daniela.scorza@uniparthenope.it

LIST OF FIGURES AND TABLES CAPTIONS

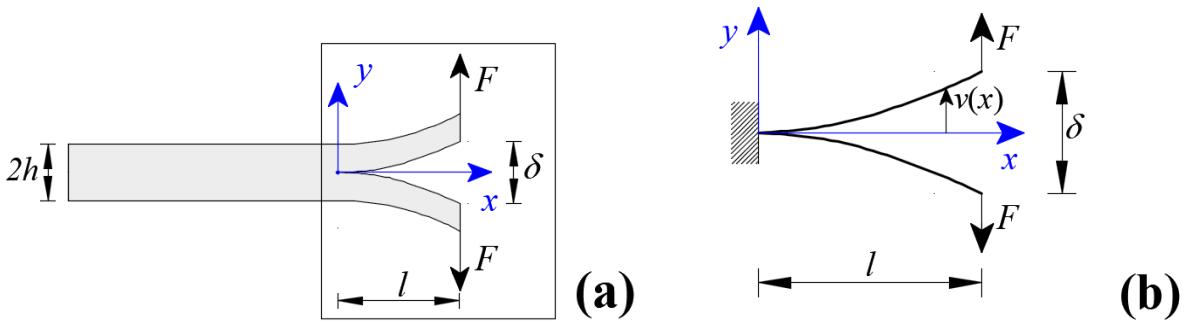

Figure 1. Edge-Cracked Nanobeam (ECN): (a) geometry and (b) double cantilever nanobeam.

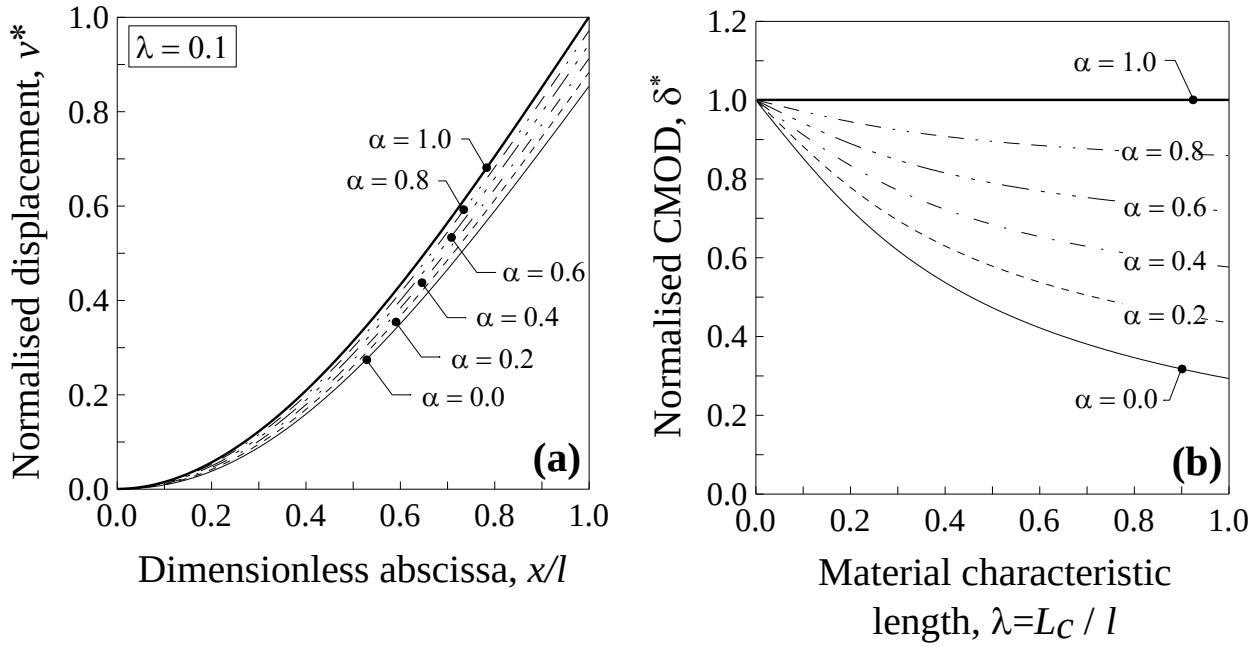

Figure 2. ECN: (a) normalised transversal displacement, v^*, against the dimensionless abscissa x/l, for the case of $\lambda = 0.1$, and (b) normalised CMOD, δ^*, against dimensionless characteristic length, λ. Six values of α are analysed.

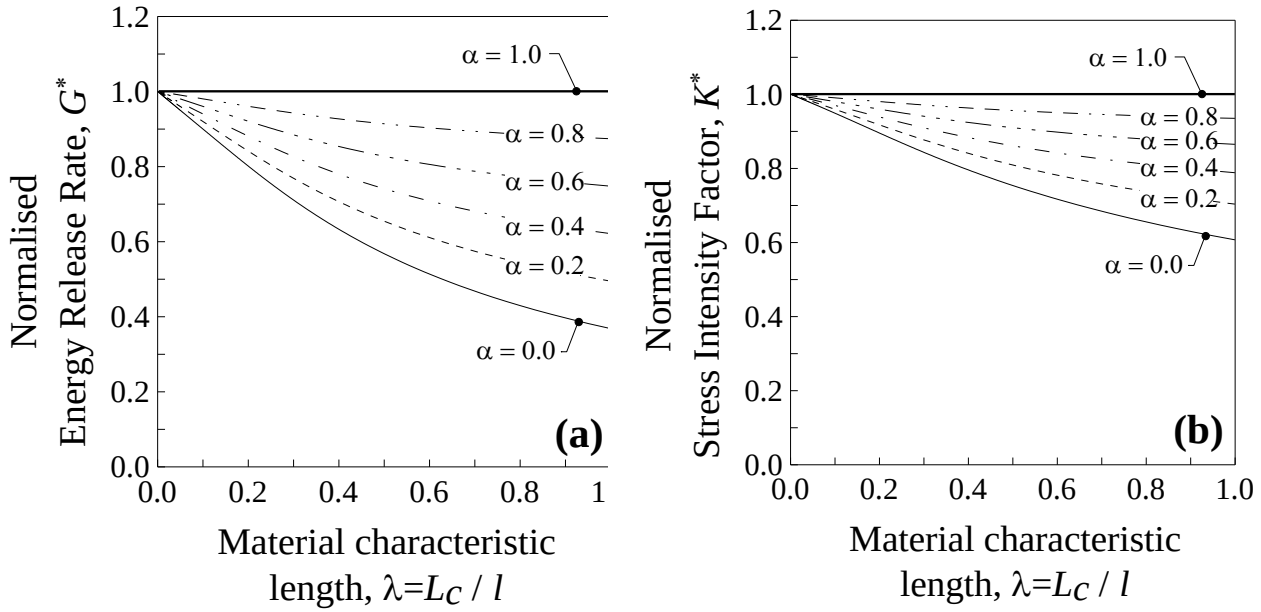

Figure 3. ECN: (a) normalised Energy Release Rate, G^*, and (b) normalised Stress Intensity Factor, K^*, against the dimensionless characteristic length, λ. Six values of α are analysed.

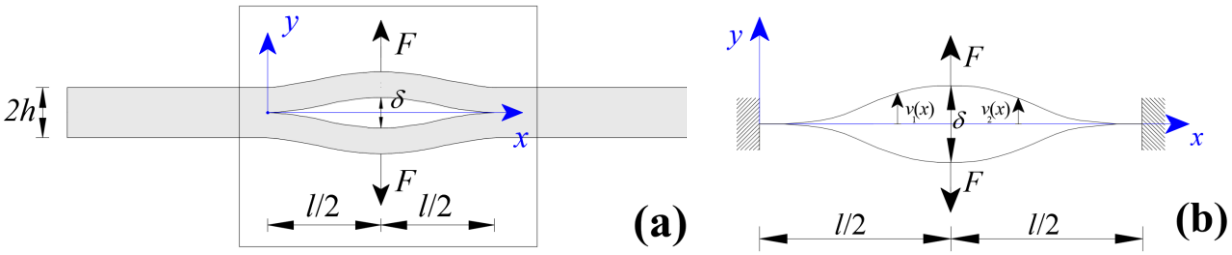

Figure 4. Centrally-Cracked Nanobeam (CCN): (a) geometry and (b) double clamped-clamped nanobeam.

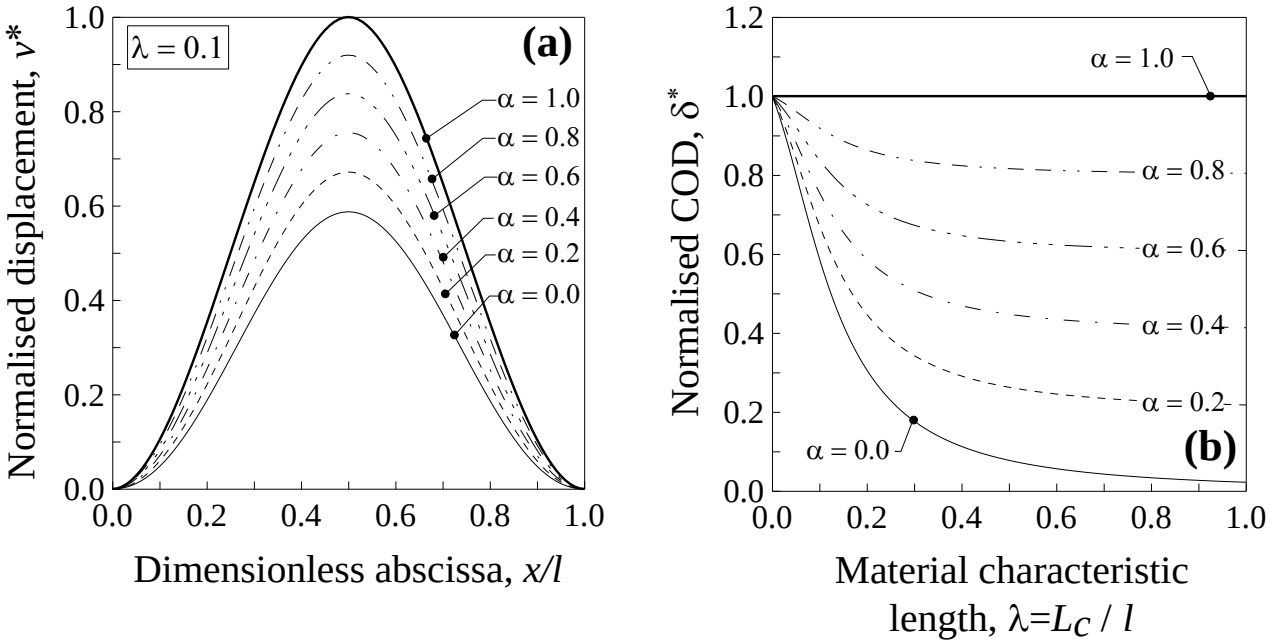

Figure 5. CCN: (a) normalised transversal displacement, v^*, against the dimensionless abscissa x/l for the case of $\lambda = 0.1$, and (b) normalised COD, δ^*, against the dimensionless characteristic length, λ. Six values of α are analysed.

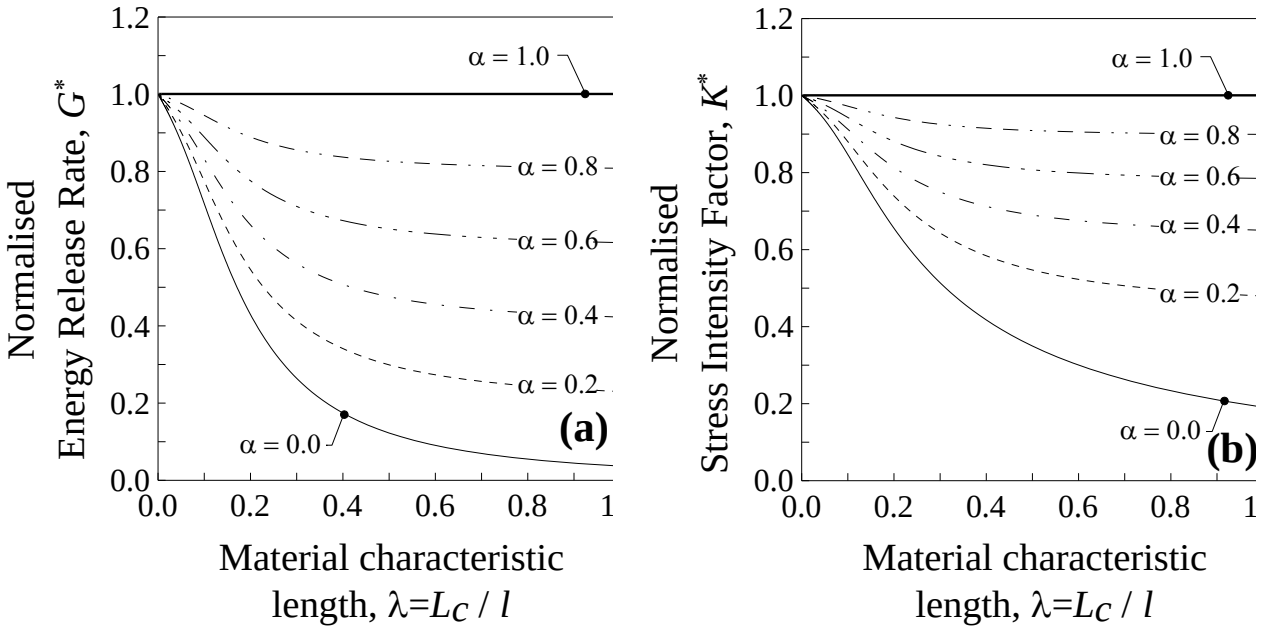

Figure 6. CCN: (a) normalised Energy Release Rate, G^*, and (b) normalised Stress Intensity Factor, K^*, against the dimensionless characteristic length, λ. Six values of α are analysed.

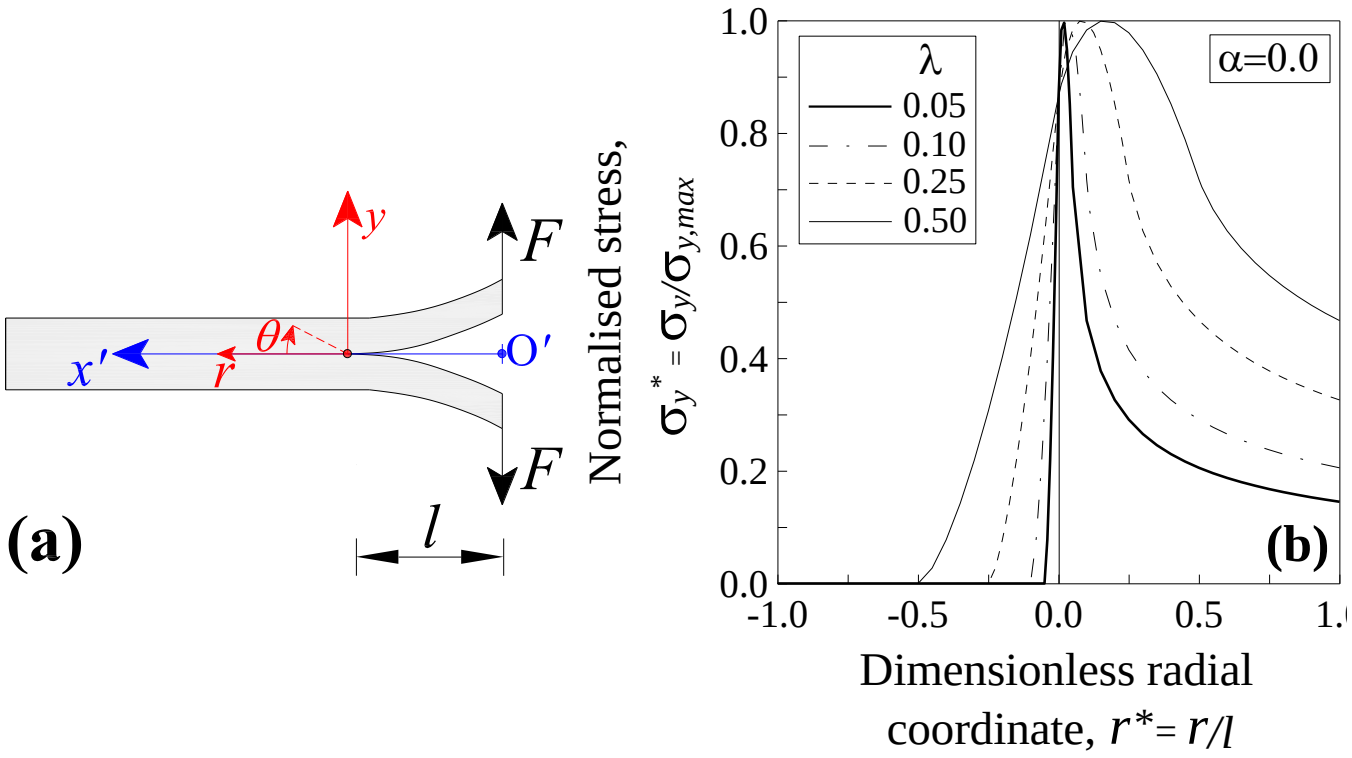

Figure 7. Stress field: a) polar reference system, and (b) normalised stress field, σ_y^*, ahead the crack tip against the dimensionless radial coordinate, r^*, for $\alpha = 0$ and four values of the dimensionless characteristic length, λ.

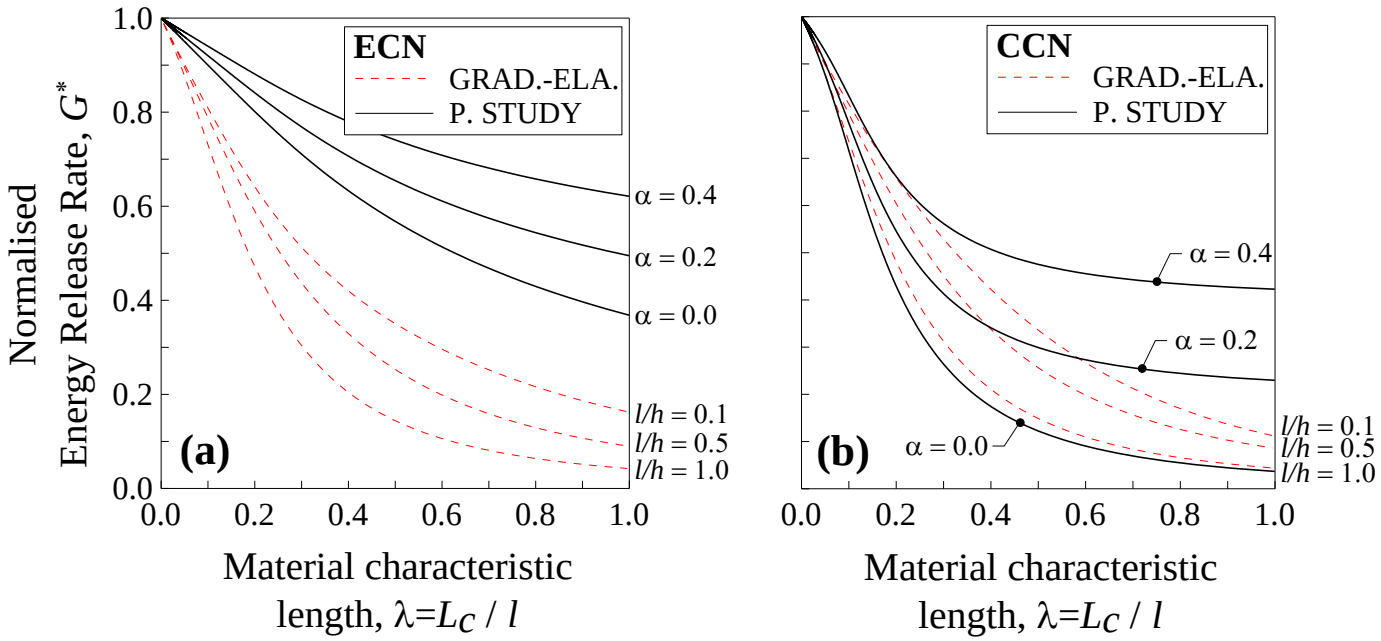

Figure 8. Comparison, in terms of ERR vs material characteristic length, λ, between the results here obtained and literature data **[54]** for both: (a) ECN and (b) CCN, by considering three values of l/h (Grad-Ela) and three value of α (local/nonlocal SDM).

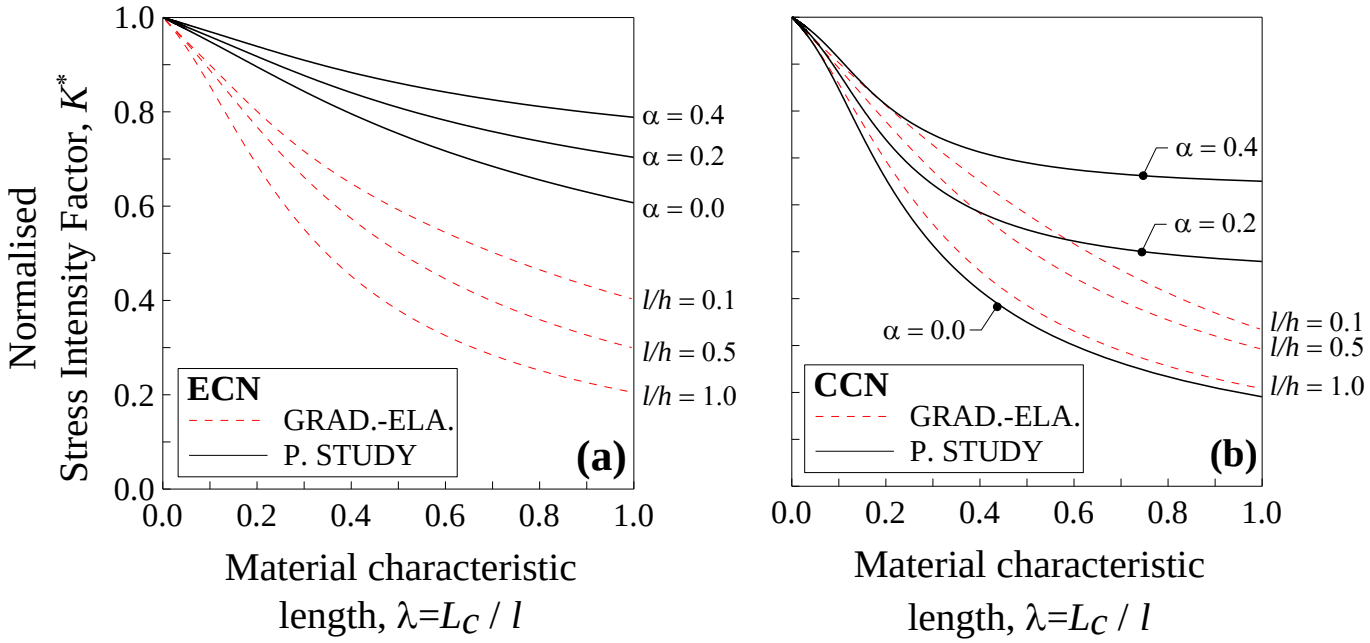

Figure 9. Comparison, in terms of SIF vs material characteristic length, λ, between the results here obtained and literature data **[54]** for both: (a) ECN and (b) CCN, by considering three values of l/h (Grad-Ela) and three value of α (local/nonlocal SDM).

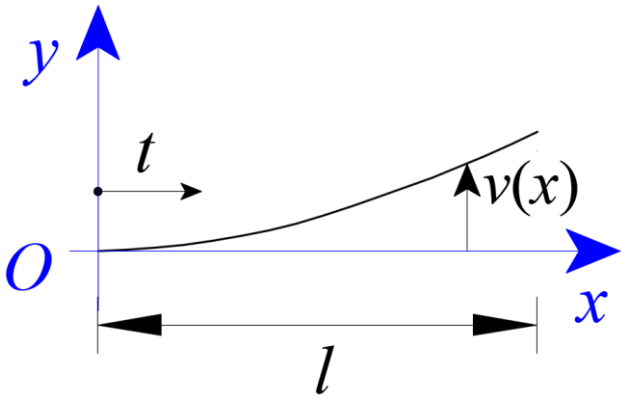

Figure A.1. Nanobeam geometry.

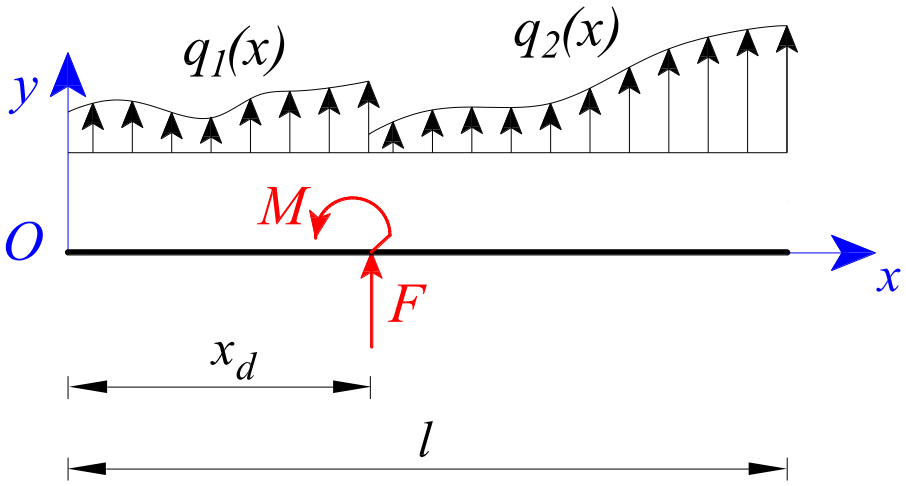

Figure A.2. Nanobeam with loading discontinuity (note that the constrains at the beam ends are not defined).